ACS APPLIED MATERIALS & INTERFACES

www.acsami.org

Research Article

Achieving Both High Ionic Conductivity and High Interfacial Stability with the $Li_{2+x}C_{1-x}B_xO_3$ Solid-State Electrolyte: Design from Theoretical Calculations

Bingkai Zhang,* Zhan Lin,* Lin-Wang Wang, and Feng Pan*

Cite This: *ACS Appl. Mater. Interfaces* 2020, 12, 6007−6014

Read Online

ACCESS | Metrics & More | Article Recommendations | Supporting Information

ABSTRACT: A crystalline solid electrolyte interphase Li_2CO_3 material with a large band gap shows promise toward next-generation all-solid-state lithium batteries (ASSLBs). However, the inferior ionic diffusivity restricts such structures to a real battery setup. Herein, based on density functional theory calculation and Python materials genomics, we theoretically develop the chemistry and local structural motifs to build a mixed boron−carbon framework $Li_{2+x}C_{1-x}B_xO_3$ (LCBO). We examine the electrochemical and chemical stabilities of LCBO-electrode interfaces by analyzing the thermodynamics of formation of interfacial phases. Interestingly, the LCBO material is automatically protected from further decomposition through the self-generated resistive interphase (Li_2CO_3 and Li_3BO_3), which gives a wide range of operating potential. LCBO shows high interfacial stability with $LiCoO_2$, $LiMnO_2$, and $LiMn_2O_4$. More importantly, the theoretical Li-ion migration barrier of LCBO (x = 0.375) is approximately 0.23 ± 0.02 eV through a cooperative migration mechanism. Therefore, the LCBO material combines high Li-ion diffusivity with good interfacial stability, which makes it a promising solid-state electrolyte material for ASSLBs.

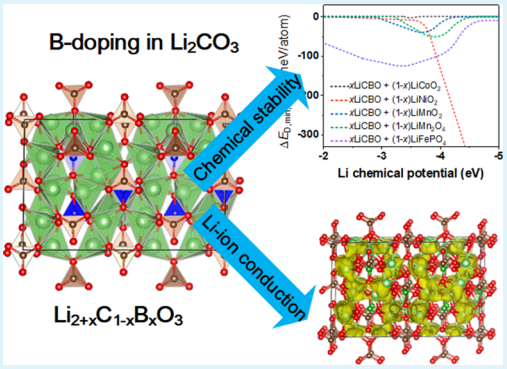

KEYWORDS: *$Li_{2+x}C_{1-x}B_xO_3$, solid electrolyte, high interfacial stability, separator, solid-state lithium battery*

1. INTRODUCTION

All-solid-state lithium batteries (ASSLBs) as potential candidates have recently been extensively studied due to their high lithium-ion (Li-ion) capacity and safety.[1−3] The most important thing in ASSLBs is the inorganic solid electrolytes (ISEs) with high ionic conductivity and good stability.[4−7] However, only a handful of crystalline structure families, such as LISICON-like,[8−10] NASICON-like,[11,12] argyrodite,[13−15] garnet,[16,17] and perovskite,[18,19] have been reported as ISEs. Finding potential solid-state electrolytes with excellent interfacial compatibility is an important task for ASSLB development.[20,21]

Li_2CO_3 is widely believed to be a solid electrolyte interphase (SEI) and is used as an artificial coating layer on electrodes due to its electrochemical stability.[22−26] Based on the properties of Li_2CO_3 coating materials, the design of crystalline Li_2CO_3 as ISEs in ASSLBs is an intriguing possibility. Other than for coating material use, experimental studies show that Li-ion conductivity in crystalline Li_2CO_3 is ∼10^{-10} S cm^{-1} (temperature = 298 K)[27] or ∼ 2 × 10^{-7} S cm^{-1} (temperature = 473 K),[28] which is far behind that of bulk ISEs (10^{-4} to 10^{-2} S cm^{-1} at room temperature).[5] The low ionic conductivity of crystalline Li_2CO_3 is due to the low intrinsic point defects such as Li interstitials since Li_2CO_3 can hardly exhibit off-stoichiometric composition on batteries. These insights motivate us to consider increasing the concentration of Li interstitials by replacing CO2-3 with BO3−3, which is $Li_{2+x}C_{1-x}B_xO_3$ (LCBO), so that it will enhance Li conductivity. Recently, Jung et al.[29] synthesized $Li_{3-x}B_{1-x}C_xO_3$ (LBCO) based on the Li_3BO_3 compound and applied the Li_3BO_3-Li_2CO_3 as coatings for the $LiCoO_2$ cathode in ASSLBs, which drastically enhances the electrochemical performances. However, the detailed LCBO phase and interfacial structures and ion conductivity are hardly investigated so far in view of ISEs.

Here, by applying the first-principles density functional theory (DFT),[30−34] ab initio molecular dynamics (AIMD),[35−39] and pymatgen materials analysis library,[40−44] we aim to probe the effect of BO3−3 units within the Li_2CO_3 framework on the phase stability, electrochemical stability, chemical stability in contact with electrodes, and ionic conductivity. These modeling and analyzing techniques are well suited to the investigation of such properties and have been applied successfully to a variety of studies on solid-state electrolytes.[45] Our results suggest that a crystalline LCBO

Received: December 7, 2019
Accepted: January 16, 2020
Published: January 16, 2020

https://dx.doi.org/10.1021/acsami.9b22185
ACS Appl. Mater. Interfaces 2020, 12, 6007−6014

material inherits good interfacial stability with electrodes from Li_2CO_3. LCBO materials have a wide electrochemical window through the formation of resistive interphase (Li_2CO_3 and Li_3BO_3) at a reduction potential of 1.27 V. LCBO also shows very high Li-ion conductivity at room temperature. Good Li-ion diffusivity and high electrochemical stability make LCBO an effective solid-state electrolyte material for ASSLBs.

2. COMPUTATIONAL METHODS

All calculations in this work were performed using Vienna ab initio simulation package (VASP).[46] The electron−ion interaction was described with the projector augmented wave (PAW).[47] Valence electrons were described using the plane wave basis set, and core electrons were kept frozen in the configuration for which the PAW dataset was generated. The electronic orbitals were expanded by plane waves with a maximum kinetic energy of 500 eV. The exchange-correlation part of the density functional was treated within the generalized gradient approximation of Perdew−Burke−Ernzerhof.[48] The convergence used for terminating the self-consistency interactions was below 10^{-6} eV/atom. For DFT simulations, a unit cell of 96 atoms with Monkhorst-Pack k-point meshes ($2 \times 2 \times 2$) was used. For AIMD simulation, a unit cell of 208 atoms with a Gamma-centered k-point mesh was used. To get more information on the DFT method, the two references (refs 49 and 50) offer more information.[49,50]

To study the thermodynamic stability upon B andC mixing with respect to the parent ternary oxide, we calculate the quantity ΔE_{mixing}, which is defined as

$$\Delta E_{mixing}(\mathrm{LCBO}) = (E(\mathrm{LCBO}) - (1-x)\cdot E(\mathrm{Li_2CO_3}) - x\cdot E(\mathrm{Li_3BO_3}))N \quad (1)$$

where N is the total number of atoms in the system. The electrochemical stability of the LCBO framework is studied using the grand potential phase diagram[43,44] and the thermochemical data in Open Quantum Materials Database (OQMD) as well as in python materials genomics (pymatgen).[51−53] The OQMD is a database of DFT-calculated thermodynamic and structural properties. We first identify the electrochemical window of the LCBO framework in a Li chemical potential range, μ_{Li}, in which the composition of LCBO is stable against either Li extraction or insertion. The μ_{Li} is determined according to the equation

$$\mu_{Li(\Phi)} = \mu 0\ \mathrm{Li} - e\Phi \quad (2)$$

where $\mu 0$ Li is the chemical potential of the Li metal, and potential Φ is open to Li.

Then, we evaluate the chemical stability of ISE-electrode interfaces to estimate whether materials react exothermically with or without the applied chemical potential.[54−56] Here, we consider the interface as a pseudobinary of the ISE and electrode, x·ISE + $(1-x)$·electrode. For LCBO-cathode interfaces at none applied potential, the mutual reaction energy is defined in terms of $\Delta E_{mutual\ energy}$ in eq 7 after considering the reaction equilibrium and the following eqs 3−6

$$\Delta E_{LCBO} = E(\mathrm{EP}) - E(\mathrm{LCBO}) \quad (3)$$

$$\Delta E_{cathode} = E(\mathrm{EP}) - E(\mathrm{Ca}) \quad (4)$$

$$E_{interface}(\mathrm{LCBO-Ca}, x) = x\cdot E(\mathrm{LCBO}) + (1-x)\cdot E(\mathrm{Ca}) \quad (5)$$

$$\Delta E_{interface}(\mathrm{LCBO-Ca}, x) = E(\mathrm{EP}, x) - E_{interface}(\mathrm{LCBO-Ca}, x) \quad (6)$$

$$\Delta E_{mutual\ energy}(\mathrm{LCBO-Ca}, x) = \Delta E_{interface}(\mathrm{LCBO-Ca}, x) - x\cdot\Delta E_{LCBO} - (1-x)\cdot\Delta E_{Ca} \quad (7)$$

where EP is the abbreviation of equilibrium phase, Ca is the abbreviation of cathode, E(EP) is determined by constructing the convex energy hull of all relevant phases in the compositional phase diagram for the corresponding LCBO or cathode, $\Delta E_{interface}$(LCBO-Ca, x) is the decomposition energy with respect to the equilibrium phase of the LCBO-Ca interface, $\Delta E_{mutual\ energy}$(LCBO-Ca, x) is the mutual energy between the LCBO and cathode interface excluding the decomposition energy of LCBO and cathode themselves. The mutual reaction energies and equations are as a function of mixing ratio at this interface x, and x varies from 0 to 1.

For LCBO-Ca interfaces at the applied lithium potentials, the decomposition mutual reaction energy is defined in terms of $\Delta E_{D,min,mutual}$ in eq 10 after considering the reaction equilibrium and the following equations:

$$\Delta E_{D,interface}(\mathrm{LCBO-Ca}, x, \Phi) = E(\mathrm{EP}, x) - E_{interface}(\mathrm{LCBO-Ca}, x) - \Delta n\cdot\mu_{Li}(\Phi) \quad (8)$$

$$\Delta E_{D,mutual}(\mathrm{LCBO-Ca}, x, \Phi) = \Delta E_{D,interface}(\mathrm{LCBO-Ca, x}, \Phi) - x\cdot\Delta E_{LCBO}(\Phi) - (1-x)\cdot\Delta E_{Ca}(\Phi) \quad (9)$$

$$\Delta E_{D,min,mutual} = \min(0 < x < 1)[\Delta E_{D,mutual}(\mathrm{LCBO-Ca}, x, \Phi)] \quad (10)$$

where $\Delta E_{D,interface}$(LCBO-Ca, x, Φ) is the decomposition energy at an applied potential, $\Delta E_{D,mutual}$(LCBO-Ca, x, Φ) is the mutual energy between LCBO and the cathode excluding the decomposition energy of LCBO and the cathode themselves, $\Delta E_{D,min,mutual}$ is minimum of the mutual reaction energy at the applied potential, and Φ here varies from 2 to 5 V.

To search for the possible Li-ion migration pathways and the corresponding migration barriers, the AIMD and climbing image nudged elastic band (Cl-NEB) methods are used.[57] Three initial images between two local energy minima structures are first set by linear interpolation and then fully relaxed. We estimate the diffusion coefficient via the following formula.

$$D_{Li} = \frac{1}{2}\nu(\Delta x)^2 e^{[-E_A/k_BT]} \quad (11)$$

where Δx is the hop distance, ν is the lattice vibrational frequency with a typical value of 10^{13} Hz, T is the temperature, and k_B is the Boltzmann constant. E_A is the migration barrier. The Li-ion conductivity (σ_{Li}) is estimated from the Nernst−Einstein relation

$$\sigma_{Li} = n_{Li}D_{Li}(q^2/k_BT) \quad (12)$$

where n_{Li} is the concentration of mobile Li ions, q is the charge of the diffusion carrier Li, k_B is the Boltzmann constant, D_{Li} is the calculated value from eq 11, and T is the temperature. In addition, the diffusion analyses are performed by using the pymatgen diffusion Python packages.[41]

3. RESULTS AND DISCUSSION

3.1. LCBO Structural Modeling. We use monoclinic Li_2CO_3 ($C2/c$ structure) to model the LCBO system, which is composed of planar CO_3 units and LiO_4 tetrahedra, as shown in Figure 1a,b. Planar CO_3 units form building blocks along the b direction. Interconnected LiO_4 tetrahedra along the bc plane are situated between these blocks. LiO_4 tetrahedra are interconnected by corner or edge sharing. After B doping, additional Li ions are introduced into the framework because of the charge compensation, shown as Li interstitials in Figure 1c,d. These Li interstitials lead to a 3D connectivity of the LiO_4 tetrahedra in LCBO. Here, the location of Li interstitials is suggested by the previous calculation. Table 1 lists the calculation results of lattice parameters for LCBO systems in

https://dx.doi.org/10.1021/acsami.9b22185
ACS Appl. Mater. Interfaces 2020, 12, 6007−6014

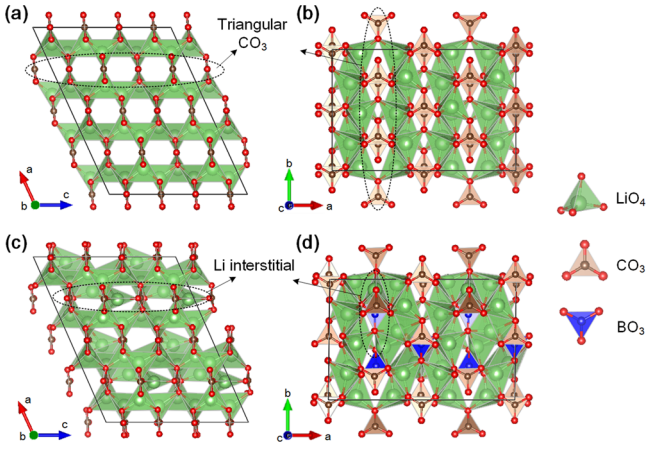

Figure 1. Polyhedral view of the Li_2CO_3 and LCBO crystal structures projected along the (a and c) *b* axis and (b and d) *c* axis. Dotted lines highlight triangular CO_3 blocks and Li interstitial. Tetrahedral LiO_4, triangular CO_3, and BO_3 units are shown in green, light brown, and light blue, respectively.

comparison with those for Li_2CO_3. The lattice constant of Li_2CO_3 is consistent with the experimental data (within 1% error). After B doping, the lattice changes are within 5%, indicating that B dopants have only a minor effect on the original structure. The density of states (DOS) of Li_2CO_3 and LCBO (in Figure S1) suggest that the LCBO system has a band gap as large as 4.4 eV. Therefore, LCBO is a good electron insulator that is potent in blocking the electron leakage and preventing electrode corrosion.

3.2. Phase Stability and Electrochemical Stability of LCBO. To study the phase stability of LCBO, we use the grand canonical linear program and explore the phase diagram of Li_2O-B_2O_3-CO_2 compounds with respect to a range of possible decomposed systems including the binary and ternary, as shown in Figure 2a. For the decomposition of LCBO, the release of CO_2 gas is not associated with a solid decomposition reaction. The only possible case is the decomposition of the quaternary LCBO ($0 < x < 0.625$) into ternary compounds, Li_2CO_3 and Li_3BO_3, with a decomposition energy from 17 to 47 meV/atom (Figure 2b). These values are much lower than those of $Li_{10}GeP_2O_{12}$ (56 meV/atom, decomposition into ternary Li_3PO_4 and Li_4GeO_4) and $Li_{10}GeP_2S_{12}$ (69 meV/atom, decomposition into ternary Li_3PS_4 and Li_4GeS_4).[40] Experiments have demonstrated the synthesis of LGPO and LGPS and success in the battery setup test.[58,59] The reason for the stability performance of them is due to the very high kinetic barrier, which prohibits the solid−solid phase decomposition. Thus, the solid decomposition is less of a problem in practice because of the kinetic obstruction. In addition, a higher B-dopant content in LCBO leads to a higher Li interstitial content but the worse stability (high decomposition energy). To balance them, we choose LCBO ($x = 0.375$) to be the optimized structure, at which point the decomposition energy is relatively close to zero while ensuring the Li interstitial content, as shown in Figure 2b.

Achieving a broad electrochemical window in ISEs is very challenging in a battery system with a high-voltage cathode and a low-voltage anode because of the extreme conditions of Li chemical potential and chemical reaction between ISEs and electrodes.[4,60] Here, the (electro)chemical stability of the LCBO system is divided into two stages: electrochemical stability and chemical stability. For electrochemical stability, using the grand potential phase diagram, we calculate the equilibrium of LCBO against a range of Li chemical potential (μ_{Li}) or voltage (Φ) to show the electrochemical stability and the voltage range where the material is stable. Figure 3 shows the electrochemical window (upper inset), phase equilibria (middle inset), and Li update versus voltage (lower inset) for the LCBO system with Li_2CO_3 and Li_3BO_3 as references. The detailed phase equilibrium at reduction and oxidation potentials of LCBO are listed in Table S1. We find that both Li_2CO_3 and Li_3BO_3 have a wide electrochemical window from reduction potentials of 1.27 and 0.30 V to oxidation potentials of 4.11 and 3.47 V (green bars in upper inset of Figure 3). For LCBO, when an applied potential range is from 1.27 to 3.47 V (yellow bar in upper inset of Figure 3), LCBO decomposes into Li_2CO_3 and Li_3BO_3 due to the voltage-induced thermodynamic driving force. However, it is noticeable that this voltage range (from 1.27 to 3.47 V) is right in the stability window of Li_2CO_3 and Li_3BO_3. The SEI-like materials can suppress the further decomposition of LCBO since Li_2CO_3 and Li_3BO_3 can block electrons and allow Li-ion transport. Therefore, the stable voltage range for LCBO is from 1.27 to 3.47 V. Recent experimental synthesis and electrochemical characterization of Li_2CO_3-Li_3BO_3 have demonstrated its phase stability and high ionic conductivity.[29] Thus, the voltage-induced instability is less problematic in practice due to the good electronic insulation and ionic conduction of Li_2CO_3-Li_3BO_3.

It is important to know whether the ISE-electrode interface reacts exothermically or whether the interface is chemically stable, which could occur in heat treatment of cell preparation or (dis)charging of cell testing. We therefore extend the above methodology to calculate the mutual reaction energy of $\Delta E_{\text{mutual energy}}$ and $\Delta E_{\text{D,min,mutual}}$ (see eqs 3−10 in the methods part), as shown in the upper and lower insets of Figure 4, respectively. The cathodes $LiXO_2$ (X = Co, Mn, and Ni), $LiFePO_4$, and $LiMn_2O_4$ are chosen as electrodes. The phase equilibria of ISE-electrode interfaces are listed in Tables S2 and S3 of the Supporting Information. In the absence of any applied chemical potential, these ISEs show good interfacial

Table 1. Experimental and Calculated Structural Parameters for Li_2CO_3 and LCBO Crystals (Space Group *C*2/*c*)

crystals	*a* (Å)	*b* (Å)	*c* (Å)	*α* (°)	*β* (°)	*γ* (°)
Li_2CO_3	8.387	5.021	6.318	90.00	114.967	90.00
Li_2CO_3 (exp.)[68]	8.359	4.974	6.194	90.00	114.789	90.00
$Li_{2.125}C_{0.875}B_{0.125}O_3$	8.412	4.982	6.413	90.523	113.193	89.732
$Li_{2.25}C_{0.75}B_{0.25}O_3$	8.468	4.986	6.501	89.821	113.012	90.132
$Li_{2.375}C_{0.625}B_{0.375}O_3$	8.443	4.978	6.603	89.556	113.697	89.753
$Li_{2.5}C_{0.5}B_{0.5}O_3$	8.404	5.013	6.793	89.945	114.073	89.687
$Li_{2.625}C_{0.375}B_{0.625}O_3$	8.381	5.012	6.696	88.267	113.543	90.263

https://dx.doi.org/10.1021/acsami.9b22185
ACS Appl. Mater. Interfaces 2020, 12, 6007−6014

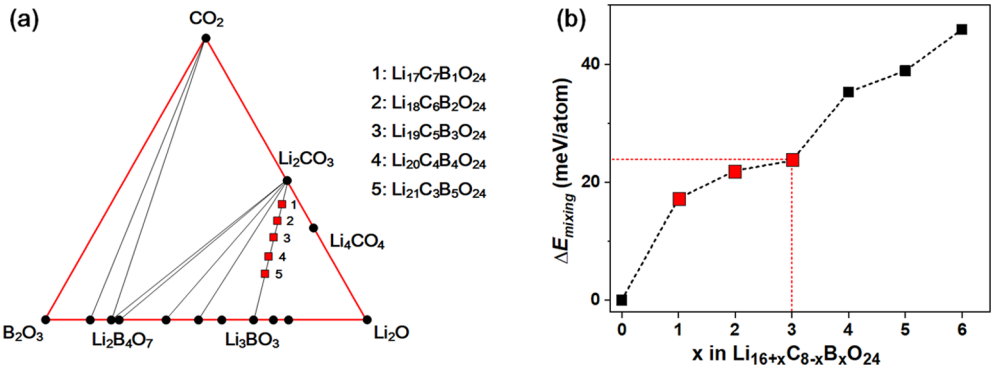

Figure 2. (a) Li-C-B-O ternary phase diagram assessing the computed stability of compounds formed by B doping in $Li_{16+x}C_{8-x}B_xO_{24}$. Results are shown in the diagram starting from stoichiometric Li_2O, Ba_2O_3, and CO_2. Black solid circles indicate clearly stable phases. Red solid squares indicate metastable phases. (b) Mixing energy in $Li_{16+x}C_{8-x}B_xO_{24}$. Cases where the mixing energy was close to zero are shown with red solid squares.

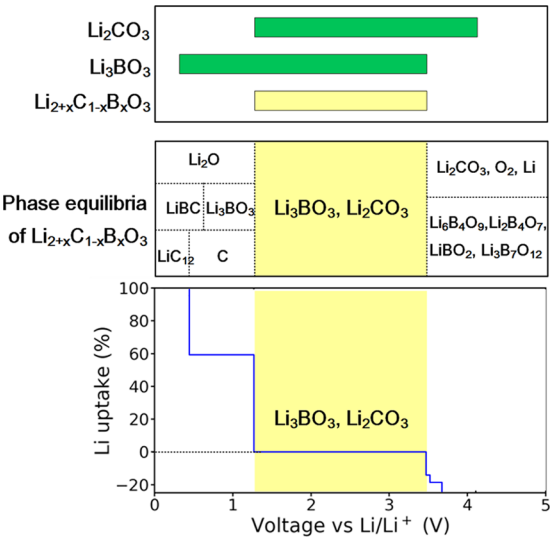

Figure 3. Electrochemical stability of studied solid electrolytes (top). Predicted phase equilibria over different voltage (μ_{Li}) ranges for LCBO (middle). Li uptake per formula unit of LCBO versus voltage (bottom). Green bars indicate stable electrochemical windows, and yellow bars indicate extended electrochemical windows.

stability with a decomposition energy from −57 to 0 meV/atom. In contrast, the decomposition energy between Li_3P_4 and $LiCoO_2$ is about −405 meV/atom. The interfaces of Li_2CO_3 with all cathodes are highly stable, and LCBO is nonreactive with $LiXO_2$. On the other hand, applying a Li chemical potential over the interfaces, the interfacial stability of ISEs is weakened with some cathodes, especially with $LiNiO_2$. The $\Delta E_{D,min,mutual}$ energy of LCBO with cathodes, except $LiFePO_4$ and $LiNiO_2$, is only in the −50 to 0 meV/atom range compared to that of garnet $Li_7La_3Zr_2O_{12}$ (LLZO) with a $LiCoO_2$ cathode (from −33 to 0 meV/atom).[55] The good stability of Li_2CO_3-Li_3BO_3 and LLZO with a $LiCoO_2$ cathode has been observed in the experiments.[29] The interfacial decomposition reactions may be kinetically inhibited. Thus, we suggest that $LiCoO_2$, $LiMnO_2$, and $LiMn_2O_4$ are suitable cathodes for LCBO, which is very helpful to improve high-voltage performance of ASSLBs. In addition, for all $\Delta E_{D,min,mutual} < 0$ interfacial reactions, the phase Li metal is in the final phase equilibria, which may lead to formation of thick interphase layers or potential degradation at the interface. Hence, further studies are presumed to evaluate their characteristics.

3.3. Li-Ion Transport in LCBO (x = 0.375). As suggested by Shi et al.,[61,62] Li-ion conductivity in Li_2CO_3 stems from the migration of intrinsic point defect (i.e., Li interstitial) and occurs through a knock-off or cooperative mechanism involving the concerted knock-off motion of interstitial and lattice lithium.[63,64] Such a cooperative migration mechanism has been elucidated in some ISEs.[52,65,66] Here, the interstitial site belongs to a LiO_4 tetrahedron and connects two parallel migration paths (along the bc plane). Then, there is a three-dimensional (3D) migration channel in LCBO.

Next, we investigate the migration of Li interstitial in LCBO. The energy profile, schematic pathways, and transition state for Li cooperative migration are shown in Figure 5. In the whole migration coordination, Li interstitial will push the neighboring lattice Li into the target interstitial site while the lattice site is filled with the original Li interstitial. The overall diffusion barrier for the Li-ion interstitial in LCBO is approximately 0.23 ± 0.02 eV; the average migration distance for each step is about 2.60 Å. For LCBO, the concentration of mobile Li ions is ∼5.54 × 10^{21} cm^{-3}. Thus, according to eqs 11−12, the calculated diffusion coefficient of D_{Li} is approximately 6.0 × 10^{-7} cm^2 s^{-1} at room temperature (300 K). Moreover, the calculated Li-ion conductivity of σ_{Li} is approximately 17 ± 10 mS cm^{-1} under room temperature. Ionic trajectories are analyzed to visualize the migration paths in Figure 6. This figure shows that Li-ion migration within this system is slightly anisotropic. Most diffusion is restricted within the LiO_4 tetrahedra layers along the bc plane with small evidence of Li-ion diffusion between layers, suggesting a quasi-isotropic three-dimensional diffusion channel. Obviously, the ionic conductivity of LCBO is superior to most of current ISE materials, such as LLZO[17] and $Li_{1+x}Al_xTi_{1-x}(PO_4)_3$.[67] Thus, LCBO is a potential ISE material in next-generation Li batteries.

4. CONCLUSIONS

In summary, by a combination of atomistic simulations and materials project database, we investigate the electrochemical properties of LCBO as a novel solid-state electrolyte. It is shown that LCBO is a good electronic insulator with a large band gap of 4.3 eV, and B doping induces slight changes on lattice parameters. Our results suggest that the stability of the LCBO phase and interface with electrodes is dependent on the

https://dx.doi.org/10.1021/acsami.9b22185
ACS Appl. Mater. Interfaces 2020, 12, 6007−6014

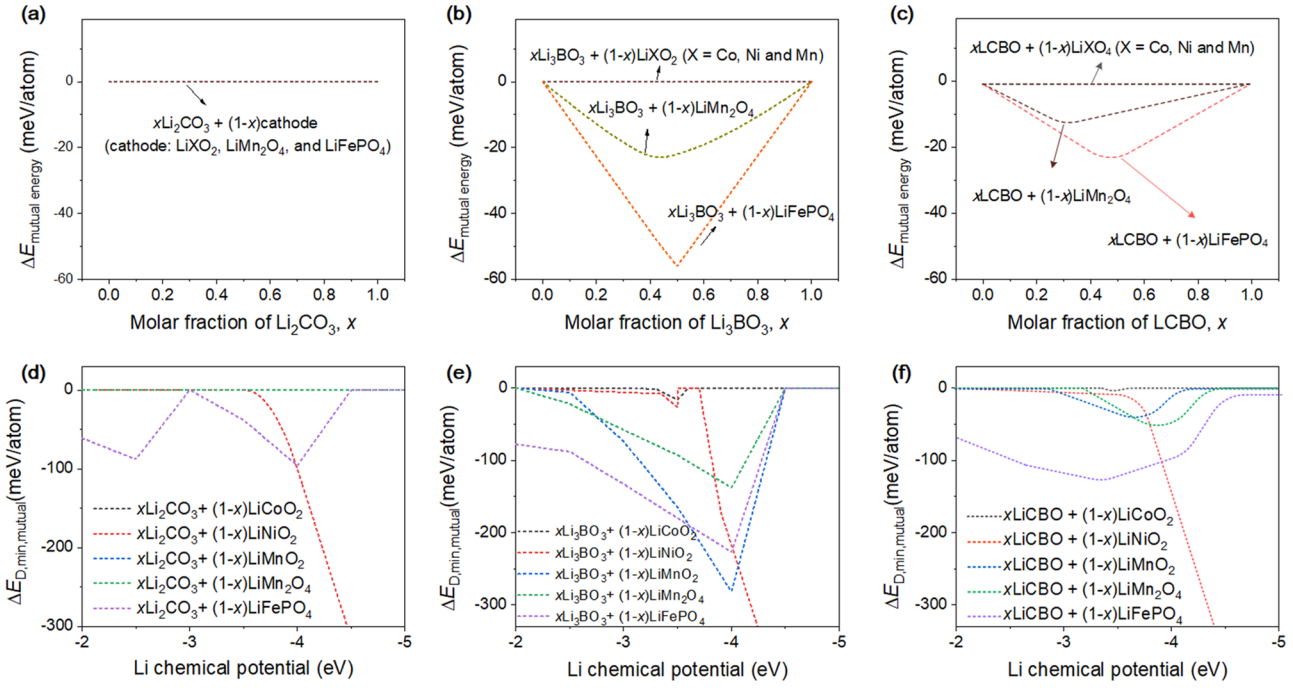

Figure 4. (a–c) Calculated mutual reaction energy $\Delta E_{mutual\ energy}$ of Li_2CO_3, Li_3BO_3, and LCBO (x = 0.375) in contact with different cathodes without any applied chemical potential. The chemical stability of interfaces in the three panels is about whether two materials would react exothermically without any applied chemical potential. (d–f) Calculated minimum mutual reaction energy $\Delta E_{D,min,mutual}$ of Li_2CO_3, Li_3BO_3, and LCBO in contact with different cathodes in which interfaces are open to different Li chemical potentials. The cathode is one of $LiXO_2$ (X = Co, Mn, and Ni), $LiFePO_4$, and $LiMn_2O_4$. Some $\Delta E_{mutual\ energy}$ and $\Delta E_{D,min,mutual}$ energies have zero or near-zero values, which overlap at the ΔE = 0. A negative value of ΔE suggests the thermodynamically favorable reaction of the interface. Therefore, the $\Delta E_{D,min,mutual}$ energy here correspondings to the most favorable decomposition energy at a ratio of x.

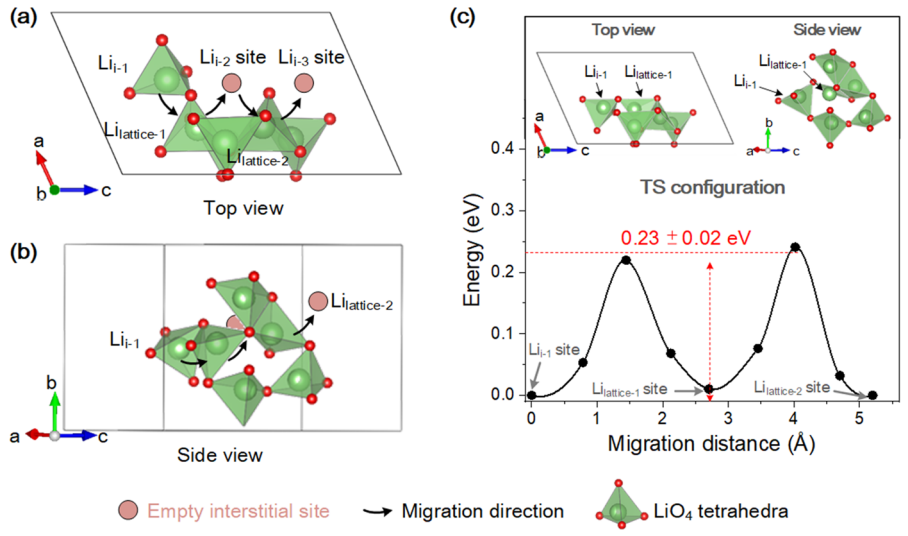

Figure 5. (a) Top and (b) side views for interconnecting LiO_4 tetrahedra arranged along the interstitial Li diffusion pathway. (c) Corresponding migration barriers (lower inset) and transition-state (TS) configuration (upper inset). Here, Li_{i-1} and Li_{i-2} are two interstitial sites, and $Li_{lattice-1}$ and $Li_{lattice-2}$ are two lattice sites. In the TS configuration, Li_{i-1}"attacks" the oxygen atoms of lattice LiO_4 tetrahedra and forms bonds with them, leading to the lattice Li-ion "departing" the same lattice LiO_4 tetrahedra.

applied voltage. The electrochemical stability studies suggest that LCBO will decompose into Li_2CO_3 and Li_3BO_3 under a voltage from 1.27 to 3.46 V. The formed phase equilibria (Li_2CO_3 and Li_3BO_3) have good electrochemical window and good chemical stability with layered $LiCoO_2$ and spinel $LiMn_2O_4$ cathodes. Meanwhile, the corresponding mutual reaction energies of LCBO with $LiCoO_2$, $LiMnO_2$, and $LiMn_2O_4$ are only in the range of −50 to 0 meV/atom, suggesting a small thermodynamic driving force. We suggest that LCBO has very good chemical stability in contact with these cathodes. Unfortunately, the phase Li metal exists in the formed phase equilibria between LCBO and cathodes, which leads to electron leakage and electrolyte corrosion. Therefore, further experimental examination is very necessary. The Li-ion cooperative migration has a migration barrier as low as 0.23 ± 0.02 eV and possesses high ionic conductivity in a quasi-

https://dx.doi.org/10.1021/acsami.9b22185
ACS Appl. Mater. Interfaces 2020, 12, 6007–6014

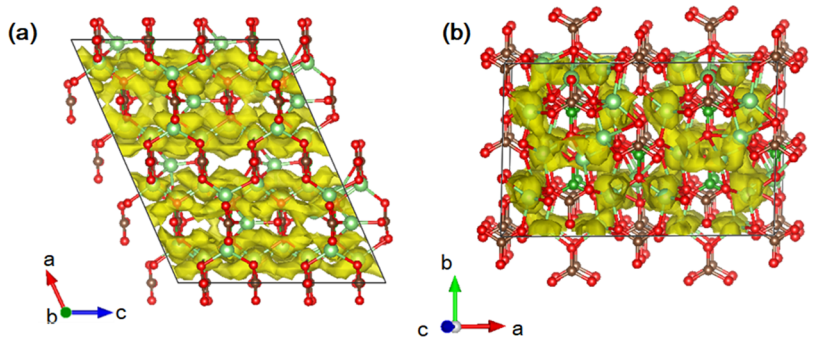

Figure 6. Isosurfaces (shown in yellow) of the ionic probability densities evaluated from ionic trajectories calculated over 60 ps AIMD at 800 K. (a) Top and (b) stereo views of the LCBO structure.

isotropic three-dimensional diffusion channel. Overall, LCBO is a potential candidate for ISE materials in ASSLBs.

■ ASSOCIATED CONTENT

Supporting Information

The Supporting Information is available free of charge at https://pubs.acs.org/doi/10.1021/acsami.9b22185.

Total density of states for Li_2CO_3 and LCBO (x = 0.375), phase equilibria at the reduction and oxidation potentials of LCBO, and electrolyte-electrode interfaces (PDF)

■ AUTHOR INFORMATION

Corresponding Authors

Bingkai Zhang − *School of Chemical Engineering and Light Industry, Guangdong University of Technology, Guangzhou 510006, China; School of Advanced Materials, Peking University Shenzhen Graduate School, Shenzhen 518055, China*; Email: zhangbk@gdut.edu.cn

Zhan Lin − *School of Chemical Engineering and Light Industry, Guangdong University of Technology, Guangzhou 510006, China*; Email: zhanlin@gdut.edu.cn

Feng Pan − *School of Advanced Materials, Peking University Shenzhen Graduate School, Shenzhen 518055, China*; orcid.org/0000-0002-8216-1339; Email: panfeng@pku.edu.cn

Author

Lin-Wang Wang − *Joint Center for Artificial Photosynthesis and Materials Sciences Division, Lawrence Berkeley National Laboratory, Berkeley, California 94720, United States*

Complete contact information is available at: https://pubs.acs.org/10.1021/acsami.9b22185

Notes

The authors declare no competing financial interest.

■ ACKNOWLEDGMENTS

This work was financially supported by startup research and development funding from the One-Hundred Young Talents Program of Guangdong University of Technology (no. 22041331901), National Key Research and Development Program of China (2016YFB0700600), Soft Science Research Project of Guangdong Province (no. 2017B030301013), Shenzhen Science and Technology Research Grant (ZDSYS201707281026184), and National Natural Science Foundation of China (no. 51703070). L.W. was supported by the Assistant Secretary for Energy Efficiency and Renewal Energy of the U.S. Department of Energy under the Battery Materials Research (BMR) program.

■ REFERENCES

(1) Armand, M.; Tarascon, J.-M. Building Better Batteries. *Nature* **2008**, *451*, 652−657.
(2) Janek, J.; Zeier, W. G. A Solid Future for Battery Development. *Nat. Energy* **2016**, *1*, 16141.
(3) Manthiram, A.; Yu, X.; Wang, S. Lithium Battery Chemistries Enabled by Solid-State Electrolytes. *Nat. Rev. Mater.* **2017**, *2*, 16103.
(4) Famprikis, T.; Canepa, P.; Dawson, J. A.; Islam, M. S.; Masquelier, C. Fundamentals of Inorganic Solid-State Electrolytes for Batteries. *Nat. Mater.* **2019**, *18*, 1278−1291.
(5) Bachman, J. C.; Muy, S.; Grimaud, A.; Chang, H.-H.; Pour, N.; Lux, S. F.; Paschos, O.; Maglia, F.; Lupart, S.; Lamp, P.; Giordano, L.; Shao-Horn, Y. Inorganic Solid-State Electrolytes for Lithium Batteries: Mechanisms and Properties Governing Ion Conduction. *Chem. Rev.* **2016**, *116*, 140−162.
(6) Yu, C.; Ganapathy, S.; van Eck, E. R. H.; Wang, H.; Basak, S.; Li, Z.; Wagemaker, M. Accessing the Bottleneck in All-Solid State Batteries, Lithium-ion Transport over the Solid-Electrolyte-Electrode Interface. *Nat. Commun.* **2017**, *8*, 1086.
(7) Zhang, B.; Tan, R.; Yang, L.; Zheng, J.; Zhang, K.; Mo, S.; Lin, Z.; Pan, F. Mechanisms and Properties of Ion-transport in Inorganic Solid Electrolytes. *Energy Storage Mater.* **2018**, *10*, 139−159.
(8) Kato, Y.; Hori, S.; Saito, T.; Suzuki, K.; Hirayama, M.; Mitsui, A.; Yonemura, M.; Iba, H.; Kanno, R. High-Power All-Solid-State Batteries using Sulfide Superionic Conductors. *Nat. Energy* **2016**, *1*, 16030.
(9) Liang, J.; Li, X.; Zhao, Y.; Goncharova, L. V.; Wang, G.; Adair, K. R.; Wang, C.; Li, R.; Zhu, Y.; Qian, Y.; Zhang, L.; Yang, R.; Lu, S.; Sun, X. In Situ Li_3PS_4 Solid-State Electrolyte Protection Layers for Superior Long-Life and High-Rate Lithium-Metal Anodes. *Adv. Mater* **2018**, *30*, 1804684.
(10) Liu, Z.; Fu, W.; Payzant, E. A.; Yu, X.; Wu, Z.; Dudney, N. J.; Kiggans, J.; Hong, K.; Rondinone, A. J.; Liang, C. Anomalous High Ionic Conductivity of Nanoporous β-Li_3PS_4. *J. Am. Chem. Soc.* **2013**, *135*, 975−978.
(11) Lang, B.; Ziebarth, B.; Elsässer, C. Lithium Ion Conduction in $LiTi_2(PO_4)_3$ and Related Compounds Based on the NASICON Structure: A First-Principles Study. *Chem. Mater.* **2015**, *27*, 5040−5048.
(12) Kahlaoui, R.; Arbi, K.; Sobrados, I.; Jimenez, R.; Sanz, J.; Ternane, R. Cation Miscibility and Lithium Mobility in NASICON $Li_{1+x}Ti_{2-x}Sc_x(PO_4)_3$ ($0 \le x \le 0.5$) Series: A Combined NMR and Impedance Study. *Inorg. Chem.* **2017**, *56*, 1216−1224.
(13) Bernges, T.; Culver, S. P.; Minafra, N.; Koerver, R.; Zeier, W. G. Competing Structural Influences in the Li Superionic Conducting Argyrodites $Li_6PS_{5-x}Se_xBr$ ($0 \le x \le 1$) upon Se Substitution. *Inorg. Chem.* **2018**, *57*, 13920−13928.

(14) Yu, C.; Ganapathy, S.; de Klerk, N. J. J.; Roslon, I.; van Eck, E. R. H.; Kentgens, A. P. M.; Wagemaker, M. Unravelling Li-ion Transport from Pico-seconds to Seconds: Bulk Versus Interfaces in an Argyrodite Li_6PS_5Cl-Li_2S All Solid State Li-ion Battery. *J. Am. Chem. Soc.* **2016**, *138*, 11192−11201.
(15) Deiseroth, H. J.; Kong, S. T.; Eckert, H.; Vannahme, J.; Reiner, C.; Zaiss, T.; Schlosser, M. Li_6PS_5X: A Class of Crystalline Li-rich Solids with an Unusually High Li^+ Mobility. *Angew. Chem., Int. Ed.* **2008**, *47*, 755−758.
(16) Jalem, R.; Rushton, M. J. D.; Manalastas, W., Jr.; Nakayama, M.; Kasuga, T.; Kilner, J. A.; Grimes, R. W. Effects of Gallium Doping in Garnet-Type $Li_7La_3Zr_2O_{12}$ Solid Electrolytes. *Chem. Mater.* **2015**, *27*, 2821−2831.
(17) Chen, Y.; Rangasamy, E.; Liang, C.; An, K. Origin of High Li^+ Conduction in Doped $Li_7La_3Zr_2O_{12}$ Garnets. *Chem. Mater.* **2015**, *27*, 5491−5494.
(18) Zhao, Y.; Daemen, L. L. Superionic Conductivity in Lithium-Rich Anti-Perovskites. *J. Am. Chem. Soc.* **2012**, *134*, 15042−15047.
(19) Deng, Z.; Radhakrishnan, B.; Ong, S. P. Rational Composition Optimization of the Lithium-Rich $Li_3OCl_{1-x}Br_x$ Anti-Perovskite Superionic Conductors. *Chem. Mater.* **2015**, *27*, 3749−3755.
(20) Tian, Y.; Shi, T.; Richards, W. D.; Li, J.; Kim, J. C.; Bo, S.-H.; Ceder, G. Compatibility Issues between Electrodes and Electrolytes in Solid-State Batteries. *Energy Environ. Sci.* **2017**, *10*, 1150−1166.
(21) Tian, Y.; Sun, Y.; Hannah, D. C.; Xiao, Y.; Liu, H.; Chapman, K. W.; Bo, S.-H.; Ceder, G. Reactivity-Guided Interface Design in Na Metal Solid-State Batteries. *Joule* **2019**, *3*, 1037−1050.
(22) Pan, J.; Zhang, Q.; Xiao, X.; Cheng, Y.-T.; Qi, Y. Design of Nanostructured Heterogeneous Solid Ionic Coatings through a Multiscale Defect Model. *ACS Appl. Mater. Interfaces* **2016**, *8*, 5687−5693.
(23) Kim, A. Y.; Strauss, F.; Bartsch, T.; Teo, J. H.; Hatsukade, T.; Mazilkin, A.; Janek, J.; Hartmann, P.; Brezesinski, T. Stabilizing Effect of a Hybrid Surface Coating on a Ni-Rich NCM Cathode Material in All-Solid-State Batteries. *Chem. Mater.* **2019**, *31*, 9664−9672.
(24) Shi, S.; Qi, Y.; Li, H.; Hector, L. G., Jr. Defect Thermodynamics and Diffusion Mechanisms in Li_2CO_3 and Implications for the Solid Electrolyte Interphase in Li-Ion Batteries. *J. Phys. Chem. C* **2013**, *117*, 8579−8593.
(25) Shi, S.; Lu, P.; Liu, Z.; Qi, Y.; Hector, L. G., Jr.; Li, H.; Harris, S. J. Direct Calculation of Li-Ion Transport in the Solid Electrolyte Interphase. *J. Am. Chem. Soc.* **2012**, *134*, 15476−15487.
(26) Li, Y.; Qi, Y. Energy Landscape of the Charge Transfer Reaction at the Complex Li/SEI/Electrolyte Interface. *Energy Environ. Sci.* **2019**, *12*, 1286−1295.
(27) Dissanayake, M. A. K. L.; Mellander, B.-E. Phase Diagram and Electrical Conductivity of the Li_2SO_4-Li_2CO_3 System. *Solid State Ionics* **1986**, *21*, 279−285.
(28) Shannon, R. D.; Taylor, B. E.; English, A. D.; Berzins, T. New Li Solid Electrolytes. *Electrochim. Acta* **1977**, *22*, 783−796.
(29) Jung, S. H.; Oh, K.; Nam, Y. J.; Oh, D. Y.; Brüner, P.; Kang, K.; Jung, Y. S. Li_3BO_3-Li_2CO_3: Rationally Designed Buffering Phase for Sulfide All-Solid-State Li-Ion Batteries. *Chem. Mater.* **2018**, *30*, 8190−8200.
(30) Richards, W. D.; Wang, Y.; Miara, L. J.; Kim, J. C.; Ceder, G. Design of $Li_{1+2x}Zn_{1-x}PS_4$, a New Lithium Ion Conductor. *Energy Environ. Sci.* **2016**, *9*, 3272−3278.
(31) Wang, Y.; Richards, W. D.; Ong, S. P.; Miara, L. J.; Kim, J. C.; Mo, Y.; Ceder, G. Design Principles for Solid-State Lithium Superionic Conductors. *Nat. Mater.* **2015**, *14*, 1026−1031.
(32) Liu, G.; Xie, D.; Wang, X.; Yao, X.; Chen, S.; Xiao, R.; Li, H.; Xu, X. High Air-Stability and Superior Lithium Ion Conduction of $Li_{3+3x}P_{1-x}Zn_xS_{4-x}O_x$ by Aliovalent Substitution of ZnO for All-Solid-State Lithium Batteries. *Energy Storage Mater.* **2019**, *17*, 266−274.
(33) Lei, X.; Wu, W.; Xu, B.; Ouyang, C.; Huang, K. LiGaOS is a Fast Li-Ion Conductor: A First-Principles Prediction. *Mater. Des.* **2020**, 108264.
(34) Yang, Y.; Wu, Q.; Cui, Y.; Chen, Y.; Shi, S.; Wang, R.-Z.; Yan, H. Elastic Properties, Defect Thermodynamics, Electrochemical Window, Phase Stability, and Li^+ Mobility of Li_3PS_4: Insights from First-Principles Calculations. *ACS Appl. Mater. Interfaces* **2016**, *8*, 25229−25242.
(35) Zhang, B.; Yang, L.; Wang, L.-W.; Pan, F. Cooperative Transport Enabling Fast Li-ion Diffusion in Thio-LISICON $Li_{10}SiP_2S_{12}$ Solid Electrolyte. *Nano Energy* **2019**, *62*, 844−852.
(36) Mo, Y.; Ong, S. P.; Ceder, G. First Principles Study of the $Li_{10}GeP_2S_{12}$ Lithium Super Ionic Conductor Material. *Chem. Mater.* **2012**, *24*, 15−17.
(37) Ong, S. P.; Mo, Y.; Richards, W. D.; Miara, L.; Lee, H. S.; Ceder, G. Phase Stability, Electrochemical Stability and Ionic Conductivity of the $Li_{10\pm1}MP_2X_{12}$ (M = Ge, Si, Sn, Al or P, and X = O, S or Se) Family of Superionic Conductors. *Energy Environ. Sci.* **2013**, *6*, 148−156.
(38) Deng, Y.; Eames, C.; Chotard, J.-N.; Lalère, F.; Seznec, V.; Emge, S.; Pecher, O.; Grey, C. P.; Masquelier, C.; Islam, M. S. Structural and Mechanistic Insights into Fast Lithium-Ion Conduction in Li_4SiO_4-Li_3PO_4 Solid Electrolytes. *J. Am. Chem. Soc.* **2015**, *137*, 9136−9145.
(39) He, X.; Zhu, Y.; Epstein, A.; Mo, Y. Statistical Variances of Diffusional Properties from *ab initio* Molecular Dynamics Simulations. *npj Comput. Mater.* **2018**, *4*, 18.
(40) Ong, S. P.; Mo, Y.; Richards, W. D.; Miara, L.; Lee, H. S.; Ceder, G. Phase stability, Electrochemical Stability and Ionic Conductivity of the $Li_{10+/-1}MP_2X_{12}$ (M = Ge, Si, Sn, Al or P, and X = O, S or Se) Family of Superionic Conductors. *Energy Environ. Sci.* **2013**, *6*, 148−156.
(41) Deng, Z.; Zhu, Z.; Chu, I.-H.; Ong, S. P. Data-Driven First-Principles Methods for the Study and Design of Alkali Superionic Conductors. *Chem. Mater.* **2017**, *29*, 281−288.
(42) Ong, S. P.; Richards, W. D.; Jain, A.; Hautier, G.; Kocher, M.; Cholia, S.; Gunter, D.; Chevrier, V. L.; Persson, K. A.; Ceder, G. Python Materials Genomics (pymatgen): A Robust, Open-Source Python Library for Materials Analysis. *Comput. Mater. Sci.* **2013**, *68*, 314−319.
(43) Ong, S. P.; Jain, A.; Hautier, G.; Kang, B.; Ceder, G. Thermal Stabilities of Delithiated Olivine MPO_4 (M=Fe, Mn) Cathodes Investigated using First Principles Calculations. *Electrochem. Commun.* **2010**, *12*, 427−430.
(44) Ong, S. P.; Wang, L.; Kang, B.; Ceder, G. Li-Fe-P-O_2 Phase Diagram from First Principles Calculations. *Chem. Mater.* **2008**, *20*, 1798−1807.
(45) Xiao, Y.; Wang, Y.; Bo, S.-H.; Kim, J. C.; Miara, L. J.; Ceder, G. Understanding Interface Stability in Solid-State Batteries. *Nat. Rev. Mater.* **2019**, 1−22.
(46) Kresse, G.; Furthmüller, J. Efficient Iterative Schemes for *ab initio* Total-energy Calculations using a Plane-wave Basis Set. *Phys. Rev. B* **1996**, *54*, 11169.
(47) Blöchl, P. E. Projector Augmented-wave Method. *Phys. Rev. B* **1994**, *50*, 17953−17979.
(48) Perdew, J. P.; Burke, K.; Ernzerhof, M. Generalized Gradient Approximation Made Simple. *Phys. Rev. Lett.* **1996**, *77*, 3865−3868.
(49) Hasnip, P. J.; Refson, K.; Probert, M. I. J.; Yates, J. R.; Clark, S. J.; Pickard, C. J. Density Functional Theory in the Solid State. *Philos. Trans. R. Soc., A* **2014**, *372*, 20130270.
(50) Meng, Y. S.; Arroyo-de Dompablo, M. E. First Principles Computational Materials Design for Energy Storage Materials in Lithium Ion Batteries. *Energy Environ. Sci.* **2009**, *2*, 589−609.
(51) Kirklin, S.; Saal, J. E.; Meredig, B.; Thompson, A.; Doak, J. W.; Aykol, M.; Rühl, S.; Wolverton, C. The Open Quantum Materials Database (OQMD): Assessing the Accuracy of DFT Formation Energies. *npj Comput. Mater.* **2015**, *1*, 15010.
(52) Monchak, M.; Hupfer, T.; Senyshyn, A.; Boysen, H.; Chernyshov, D.; Hansen, T.; Schell, K. G.; Bucharsky, E. C.; Hoffmann, M. J.; Ehrenberg, H. Lithium Diffusion Pathway in $Li_{1.3}Al_{0.3}Ti_{1.7}(PO_4)_3$ (LATP) Superionic Conductor. *Inorg. Chem.* **2016**, *55*, 2941−2945.

https://dx.doi.org/10.1021/acsami.9b22185
ACS Appl. Mater. Interfaces 2020, 12, 6007−6014

(53) Nolan, A. M.; Zhu, Y.; He, X.; Bai, Q.; Mo, Y. Computation-Accelerated Design of Materials and Interfaces for All-Solid-State Lithium-Ion Batteries. *Joule* **2018**, *2*, 2016−2046.
(54) Han, F.; Zhu, Y.; He, X.; Mo, Y.; Wang, C. Electrochemical Stability of $Li_{10}GeP_2S_{12}$ and $Li_7La_3Zr_2O_{12}$ Solid Electrolytes. *Adv. Energy Mater.* **2016**, *6*, 1501590.
(55) Zhu, Y.; He, X.; Mo, Y. First principles study on electrochemical and chemical stability of solid electrolyte−electrode interfaces in all-solid-state Li-ion batteries. *J. Mater. Chem. A* **2016**, *4*, 3253−3266.
(56) Zhu, Y.; He, X.; Mo, Y. Origin of Outstanding Stability in the Lithium Solid Electrolyte Materials: Insights from Thermodynamic Analyses Based on First-Principles Calculations. *ACS Appl. Mater. Interfaces* **2015**, *7*, 23685−23693.
(57) Henkelman, G.; Uberuaga, B. P.; Jónsson, H. A Climbing Image Nudged Elastic Band Method for Finding Saddle Points and Minimum Energy Paths. *J. Chem. Phys.* **2000**, *113*, 9901−9904.
(58) Song, S.; Dong, Z.; Deng, F.; Hu, N. Lithium Superionic Conductors $Li_{10}MP_2O_{12}$ (M = Ge, Si). *Funct. Mater. Lett.* **2018**, *11*, 1850039.
(59) Kamaya, N.; Homma, K.; Yamakawa, Y.; Hirayama, M.; Kanno, R.; Yonemura, M.; Kamiyama, T.; Kato, Y.; Hama, S.; Kawamoto, K.; Mitsui, A. A Lithium Superionic Conductor. *Nat. Mater.* **2011**, *10*, 682−686.
(60) Fitzhugh, W.; Wu, F.; Ye, L.; Deng, W.; Qi, P.; Li, X. A High-Throughput Search for Functionally Stable Interfaces in Sulfide Solid-State Lithium Ion Conductors. *Adv. Energy Mater.* **2019**, *9*, 1900807.
(61) Shi, S.; Lu, P.; Liu, Z.; Qi, Y.; Hector, L. G., Jr.; Li, H.; Harris, S. J. Direct Calculation of Li-ion Transport in the Solid Electrolyte Interphase. *J. Am. Chem. Soc.* **2012**, *134*, 15476−15487.
(62) Shi, S.; Qi, Y.; Li, H.; Hector, L. G., Jr. Defect Thermodynamics and Diffusion Mechanisms in Li_2CO_3 and Implications for the Solid Electrolyte Interphase in Li-ion Batteries. *J. Phys. Chem. C* **2013**, *117*, 8579−8593.
(63) He, X.; Zhu, Y.; Mo, Y. Origin of Fast Ion Diffusion in Super-ionic Conductors. *Nat. Commun.* **2017**, *8*, 15893.
(64) Zhang, B.; Yang, L.; Wang, L.-W.; Pan, F. Cooperative Transport Enabling Fast Li-ion Diffusion in Thio-LISICON $Li_{10}SiP_2S_{12}$ Solid Electrolyte. *Nano Energy* **2019**, *62*, 844−852.
(65) Zhang, Z.; Zou, Z.; Kaup, K.; Xiao, R.; Shi, S.; Avdeev, M.; Hu, Y.-S.; Wang, D.; He, B.; Li, H.; Huang, X.; Nazar, L. F.; Chen, L. Correlated Migration Invokes Higher Na^+-Ion Conductivity in NaSICON-Type Solid Electrolytes. *Adv. Energy Mater.* **2019**, *9*, 1902373.
(66) Zhang, B.; Lin, Z.; Dong, H.; Wang, L.-W.; Pan, F. Revealing Cooperative Li-ion Migration in $Li_{1+x}Al_xTi_{2-x}(PO_4)_3$ Solid State Electrolytes with High Al Doping. *J. Mater. Chem. A* **2020**, *8*, 342−348.
(67) Deng, Z.; Mo, Y.; Ong, S. P. Computational Studies of Solid-state Alkali Conduction in Rechargeable Alkali-ion Batteries. *NPG Asia Mater.* **2016**, *8*, No. e254.
(68) Idemoto, Y.; Richardson, J. W., Jr.; Koura, N.; Kohara, S.; Loong, C.-K. Crystal Structure of $(Li_xK_{1-x})_2CO_3$ (x = 0, 0.43, 0.5, 0.62, 1) by Neutron Powder Diffraction Analysis. *J. Phys. Chem. Solids* **1998**, *59*, 363−376.

https://dx.doi.org/10.1021/acsami.9b22185
ACS Appl. Mater. Interfaces 2020, 12, 6007−6014